[1] **V. I. Gnesin**, Doctor of Technical Sciences
[2] **L. V. Kolodiazhnaya**, Doctor of Technical Sciences
[2] **R. Rzadkowski**, Doctor of Technical Sciences

[1] A. Podgorny Institute of Mechanical Engineering Problems of NASU, Kharkiv, Ukraine,
e-mail: gnesin@ukr.net
[2] The Szewalski Institute of Fluid-Flow Machinery PAS, Gdansk, Poland,
e-mail: z3@imp.gda.pl

Ключові слова: *аеропружна поведінка, в'язкий потік, лопатковий вінець, автоколивання, зв'язана задача, нестаціонарне навантаження.*

UDC 621.165

AEROELASTIC BEHAVIOUR OF TURBINE BLADE ROW IN 3D VISCOUS FLOW

Наведено результати чисельного аналізу аеропружної поведінки вібруючого лопаткового вінця турбінного ступеня в тривимірному потоці в'язкого газу з урахуванням нерівномірного розподілу тиску в окружному напрямі за лопатковим вінцем. Чисельний метод ґрунтується на розв'язанні зв'язаної задачі нестаціонарної аеродинаміки та пружних коливань лопаток в нестаціонарному просторовому потоці газу через лопатковий вінець останнього ступеня осьової турбіни. Наведений метод дозволяє прогнозувати амплітудно-частотний спектр коливань лопаток у потоці газу, включаючи вимушені та самозбудні коливання (флатер чи автоколивання).

Introduction

The necessity to simulate complex and off-design modes of turbo-machinery flows requires the use of Navier-Stokes equations to overcome the limitations connected with the non-viscous mode [1].

In the present study, the 3D Reynolds-averaged Navier-Stokes equations (RANS), coupled with modified Baldwin-Lomax algebraic eddy viscosity turbulence model, is applied to calculate 3D unsteady viscous flow through the oscillating blade row [2].

The approach is based on the solution of the coupled aerodynamic-structure problem for the 3D flow through the turbine blade row in which both fluid and dynamic equations are integrated simultaneously in time, thus providing the correct formulation of the coupled problem, as the blade oscillations and loads acting on the blades are part of the solution [1, 3 – 7].

The paper presents the numerical results of the turbine blade row aeroelastic characteristics and aerodamping coefficients under the given harmonic and coupled blade oscillations, taking into consideration the 1st natural mode at different inter-blade phase angles of blade oscillations (IBPA = 0 deg; ± 90 deg; 180 deg.).

The calculation results showed the stable aerodamping of oscillations at different shift phase angles of blade oscillations.

Problem formulation

A 3D unsteady flow of viscous compressible gas through an isolated turbine blade row of oscillating blades is considered. The turbine blade row is as annular cascade consisting of 53 blades. The problem of gas flow through the turbine blade row is based on the assumption that blade oscillations are performed with a constant inter-blade phase angle (IBPA). The flow from blade to blade is assumed to be aperiodic as the calculated domain includes the number of blades depending on IBPA.

In this work, the blade motion is considered with the use of a modal approach, in which the blade motion is assumed to be the linear superposition of the natural modes of blade oscillations with modal coefficients changing in accordance with the given harmonic law

$$u_j(x,t) = \sum_{i=1}^{N} \{U_i(x)\}\, q_{ij}(t),$$

$$q_{ij} = q_{0i} \cdot \sin\left[2\pi\nu t + (j-1)\theta_i\right],$$

where $\{U_i(x)\}$ – is the displacement vector corresponding to the i^{th} natural mode; $q_{ij}(t)$ is the modal coefficient corresponding to the i^{th} oscillation mode for the j^{th} blade; q_{0i} is the dimensional factor; θ_i is the phase angle.

3D viscous gas transonic flow is considered to be in the physical domain including the blade row rotating with a constant angular velocity and is described by unsteady 3D Reynolds-averaged Navier-Stokes equations, presented in the form of integral conservation laws

$$\frac{\partial}{\partial t}\int\limits_{\Omega} U\, d\Omega + \oint\limits_{\sigma} \overline{F}\cdot\overline{n}\, d\sigma = \int\limits_{\sigma} \overline{R}\cdot\overline{n}\, d\sigma\,. \tag{1}$$

Values $\overline{F}$ and $\overline{R}$, symbolic vectors of non-viscous and viscous flows in a Cartesian system of coordinates for the hexahedral finite volume with the normal to the lateral surface $\vec{n}(\alpha_i, \beta_i, \gamma_i)$ $(i = 1, 3)$, are presented as follows:

$$\left(\overline{F}\cdot\overline{n}\right) = \left(F_1, F_2, F_3\right);\ \left(\overline{R}\cdot\overline{n}\right) = \left(R_1, R_2, R_3\right);$$

$$F_1 = \begin{pmatrix} \rho\left(\upsilon_1\alpha_1 + \upsilon_2\beta_1 + \upsilon_3\gamma_1\right) \\ \rho\,\upsilon_1\left(\upsilon_1\alpha_1 + \upsilon_2\beta_1 + \upsilon_3\gamma_1\right) + p\,\alpha_1 \\ \rho\,\upsilon_2\left(\upsilon_1\alpha_1 + \upsilon_2\beta_1 + \upsilon_3\gamma_1\right) + p\,\beta_1 \\ \rho\,\upsilon_3\left(\upsilon_1\alpha_1 + \upsilon_2\beta_1 + \upsilon_3\gamma_1\right) + p\,\gamma_1 \\ \left(h + p\right)\left(\upsilon_1\alpha_1 + \upsilon_2\beta_1 + \upsilon_3\gamma_1\right) \end{pmatrix};\ F_2 = \begin{pmatrix} \rho\left(\upsilon_1\alpha_2 + \upsilon_2\beta_2 + \upsilon_3\gamma_2\right) \\ \rho\,\upsilon_1\left(\upsilon_1\alpha_2 + \upsilon_2\beta_2 + \upsilon_3\gamma_2\right) + p\,\alpha_2 \\ \rho\,\upsilon_2\left(\upsilon_1\alpha_2 + \upsilon_2\beta_2 + \upsilon_3\gamma_2\right) + p\,\beta_2 \\ \rho\,\upsilon_3\left(\upsilon_1\alpha_2 + \upsilon_2\beta_2 + \upsilon_3\gamma_2\right) + p\,\gamma_2 \\ \left(h + p\right)\left(\upsilon_1\alpha_2 + \upsilon_2\beta_2 + \upsilon_3\gamma_2\right) \end{pmatrix};$$

$$F_3 = \begin{pmatrix} \rho\left(\upsilon_1\alpha_3 + \upsilon_2\beta_3 + \upsilon_3\gamma_3\right) \\ \rho\,\upsilon_1\left(\upsilon_1\alpha_3 + \upsilon_2\beta_3 + \upsilon_3\gamma_3\right) + p\,\alpha_3 \\ \rho\,\upsilon_2\left(\upsilon_1\alpha_3 + \upsilon_2\beta_3 + \upsilon_3\gamma_3\right) + p\,\beta_3 \\ \rho\,\upsilon_3\left(\upsilon_1\alpha_3 + \upsilon_2\beta_3 + \upsilon_3\gamma_3\right) + p\,\gamma_3 \\ \left(h + p\right)\left(\upsilon_1\alpha_3 + \upsilon_2\beta_3 + \upsilon_3\gamma_3\right) \end{pmatrix},$$

$$R_1 = \begin{pmatrix} 0 \\ \tau_{xx}\alpha_1 + \tau_{xy}\beta_1 + \tau_{xz}\gamma_1 \\ \tau_{yx}\alpha_1 + \tau_{yy}\beta_1 + \tau_{yz}\gamma_1 \\ \tau_{zx}\alpha_1 + \tau_{zy}\beta_1 + \tau_{zz}\gamma_1 \\ \beta_x\alpha_1 + \beta_y\beta_1 + \beta_z\gamma_1 \end{pmatrix};\ R_2 = \begin{pmatrix} 0 \\ \tau_{xx}\alpha_2 + \tau_{xy}\beta_2 + \tau_{xz}\gamma_2 \\ \tau_{yx}\alpha_2 + \tau_{yy}\beta_2 + \tau_{yz}\gamma_2 \\ \tau_{zx}\alpha_2 + \tau_{zy}\beta_2 + \tau_{zz}\gamma_2 \\ \beta_x\alpha_2 + \beta_y\beta_2 + \beta_z\gamma_2 \end{pmatrix};$$

$$R_3 = \begin{pmatrix} 0 \\ \tau_{xx}\alpha_3 + \tau_{xy}\beta_3 + \tau_{xz}\gamma_3 \\ \tau_{yx}\alpha_3 + \tau_{yy}\beta_3 + \tau_{yz}\gamma_3 \\ \tau_{zx}\alpha_3 + \tau_{zy}\beta_3 + \tau_{zz}\gamma_3 \\ \beta_x\alpha_3 + \beta_y\beta_3 + \beta_z\gamma_3 \end{pmatrix}.$$

Here p is pressure, ρ is density, τ is tangential stress, and υ_1, υ_2, υ_3 are velocity components.

The calculated domain includes all the blades on the whole annulus of the inlet and outlet domains and is divided into the finite number of linear hexahedral elements. These elements are assumed to cover the whole computational domain. Subdivision of the domain into the hexahedral elements makes it possible to use indices *i, j, k*.

A 3D grid consists of a sequence of 2D grids that are stacked together in the radial direction (from hub to tip). The 2D grids at each radial location are similar and each of them is divided into different segments. Each of the segments includes a blade and has a spread in the circumferential direction, which is equal to the blade pitch. In turn, each of the segments is discretized using a hybrid H-O grid. The meridional

section of the calculated domain is shown in Fig. 1. The root, middle, and peripheral sections of the blade, as well as the 2D hybrid H-O grids for these sections are presented in Fig. 2.

The calculations were performed using a structural hybrid H-O grid consisting of 210,960 cells in each channel, including the moving O-grid consisting of 165,600 cells.

The geometrical and gas-dynamic parameters for each channel are described in a Cartesian system of coordinates *x, y, z*, fixed rigidly with the static (in equilibrium) position of each blade. Axis *x* is in the radial direction of a blade, axis *z* is oriented along the axis of the blade rotation, and axis *y* corresponds to the blade's circumferential direction, so that axes *x, y, z* form a right-handed coordinate system (Fig. 2).

The system of equations is integrated with the Godunov-Kolgan difference scheme of the second-order of accuracy with respect to the spatial coordinates of the moving grid.

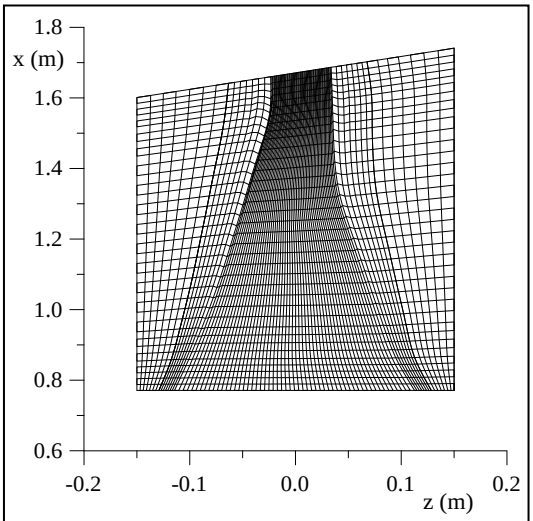

Fig 1. Meridional section of difference grid

The unsteady effects on the blade row were assumed to be caused by the rotor blade rotation in the unsteady flow and blade oscillations under the influence of unsteady aerodynamic loads. The formulation of the boundary conditions at the channel inlet and outlet is based on the one-dimensional theory of characteristics.

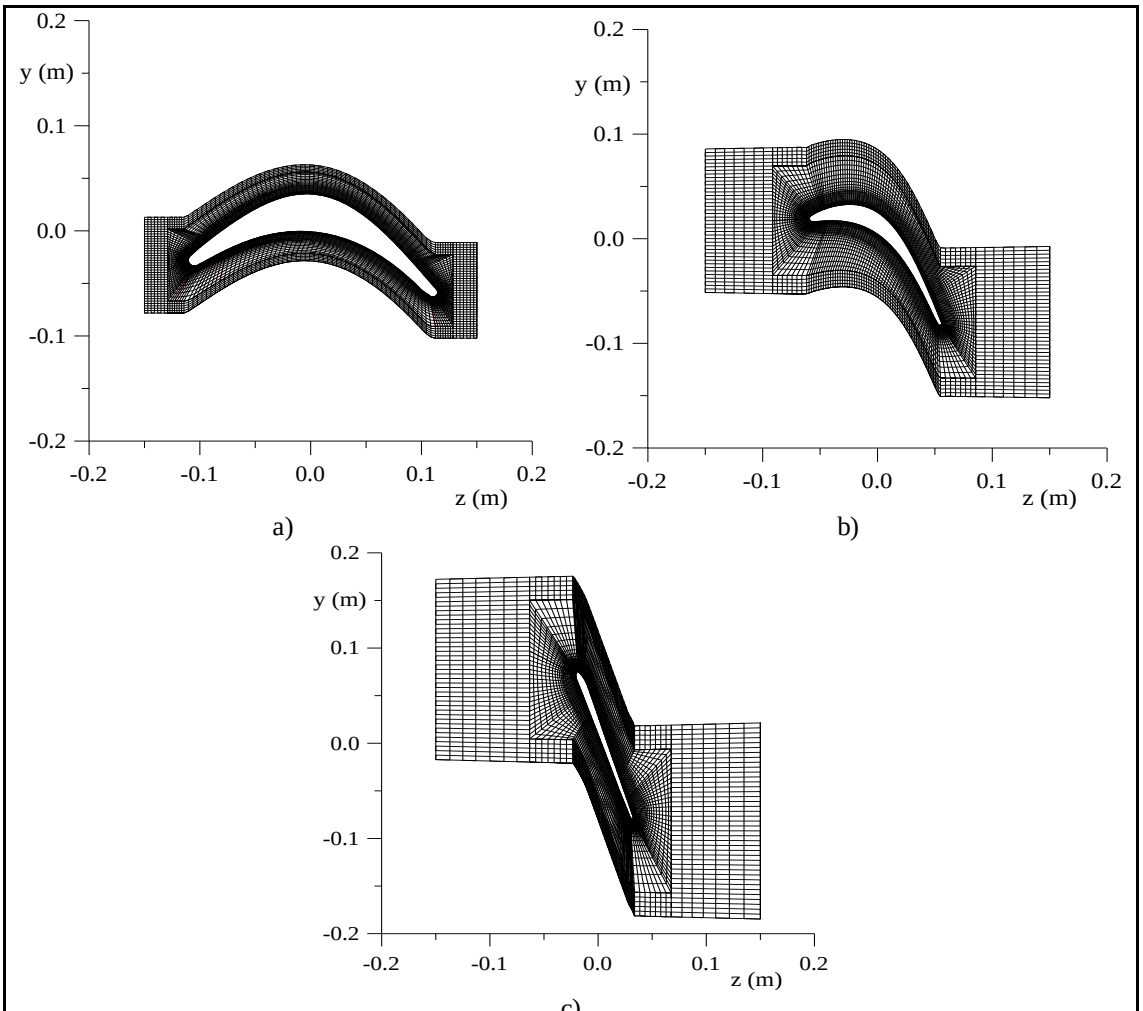

Fig. 2. Difference grid:
a) – root sections; b) – middle sections; c) – peripheral sections

Generally, if the axial velocity is subsonic, the complete system of the boundary conditions can be presented:

– before the blade row, or at its inlet, as

$$T_0 = T_0(x, y); \quad P_0 = P_0(x, y); \quad \alpha = \alpha(x, y); \; \gamma = \gamma(x, y); \quad d\left(\upsilon_3 - \frac{2a}{\lambda - 1}\right) = 0,$$

– behind the blade row, or at its outlet, as

$$p = p(x, y); dp - a^2 dp = 0; d\upsilon_1 - \left(\omega^2 r - 2\omega\upsilon_2\right) dt = 0 \; ,$$

$$d\upsilon_2 + 2\omega\upsilon_1 dt = 0; \; d\left(\upsilon_3 + \frac{2a}{\lambda - 1}\right) = 0 \, .$$

Here T_0, P_0 are the total temperature and pressure in the absolute coordinate system, α, γ are the flow angles in the tangential and meridional directions at the blade row inlet; p is the static pressure at the blade row outlet.

The discrete form of equations (1) is built for an arbitrary space deforming difference grid as

$$\frac{1}{2\Delta t}[3U^{n+1}\Omega^{n+1} - 4U_n\Omega_n + U_{n-1}\Omega_{n-1}] + \left[\left(-U w_n + F_1 - R_1\right)\sigma\right]_{i+1} - \left[\left(-U w_n + F_1 - R_1\right)\sigma\right]_i +$$

$$+ \left[\left(-U w_n + F_2 - R_2\right)\sigma\right]_{j+1} - \left[\left(-U w_n + F_2 - R_2\right)\sigma\right]_j +$$

$$+ \left[\left(-U w_n + F_3 - R_3\right)\sigma\right]_{k+1} - \left[\left(-U w_n + F_3 - R_3\right)\sigma\right]_k + H_n\Omega_n = 0 \, .$$

Here the lower and upper indices correspond to the 'old' and 'new' sells, $f = \{\rho, \rho\vec{\upsilon}, E\}$ is a symbolical vector of conservative variables, F_1, F_2, F_3 are the flows of conservative variables through lateral faces, σ and w_n are the square and normal velocity of a lateral face centre. The gas-dynamic parameters on the lateral faces are defined from the solution to the Riemann problem of breakdown of an arbitrary discontinuity.

The dynamical model of a vibrating blade is described by the matrix equation

$$[M]\{\ddot{u}(x,t)\} + [C]\{\dot{u}(x,t)\} + [K]\{u(x,t)\} = [F], \tag{2}$$

where [M], [C] and [K] are matrices of mass, mechanical damping, and stiffness of a blade; $\{u(x, t)\}$ is the blade displacement; [F] is the vector of unsteady aerodynamic loads.

Using the modal approach

$$\{\, u(x,t) \,\} = [U(x)]\{\, q(t) \,\} = \sum_{i=1}^{N} \{U_i(x)\} q_i(t),$$

where $U_i(x)$ is the blade displacement vector by i-mode; $q_i(t)$ is a modal coefficient of i-mode, and, taking into account the orthogonality of natural modes, matrix equation (2) is reduced to a system of ordinary differential equations relative to modal coefficients of natural modes

$$\ddot{q}_i(t) + 2h_i\dot{q}_i(t) + \omega_i^2 q_i(t) = \lambda_i(t). \tag{3}$$

Here h_i is the mechanical damping coefficient of i-mode; ω_i is the natural frequency of i-mode; λ_i is the modal force corresponding to the blade displacement by i-mode, calculated in each iteration in response to the pressure distribution along the surface of a blade

$$\lambda_i = \frac{\iint\limits_{\sigma} p\overline{U}_i \cdot \overline{n}^{\circ} \, d\sigma}{\iiint\limits_{v} \rho \overline{U}_i^2 \, dv},$$

Having defined the modal coefficients from the system (3), we receive the displacement and velocity of a blade as

$$u(x,t) = \sum_i U_i(x) q_i(t),$$

$$\dot{u}(x,t) = \sum_i U_i(x) \dot{q}_i(t).$$

The block diagram for calculating n – iterations in an aeroelastic model can be presented as

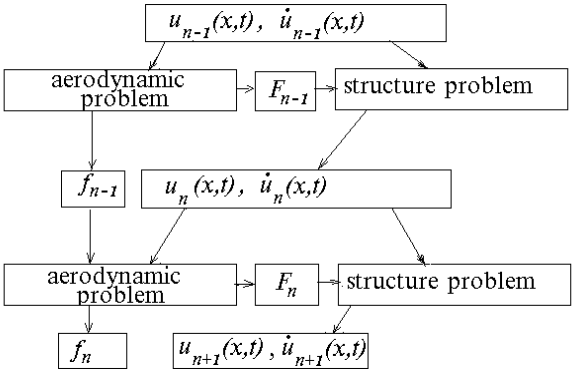

Numerical analysis

The numerical investigation was performed for a turbine rotor blade row consisting of 53 blades .

The boundary conditions at inlet and outlet were accepted as follows:

− the total pressure in an absolute system of coordinates P_0 = 37840÷38670 Pa, (Fig. 3);

− the total temperature in an absolute system T_0 = 348 °K;

− flow angles in an absolute system of coordinates in the radial and circumferential directions were given;

− the static pressure at the blade row outlet P_2 = 10410÷10830 Pa (Fig. 3).

The graphs of the total pressure in an absolute system of coordinates (P_0), in a relative rotating system (P_{0w}) and of the static pressure at the blade row outlet are shown in Fig. 3.

In Fig. 4 is shown the static pressure distribution at the blade row outlet in the circumferential direction. The curve on Fig. 4, a corresponds to the pressure distribution in the root section behind the blade row, in Fig. 4, b – in the middle section, and in Fig. 4, c – in the peripheral section.

The aerodynamic calculations of gas flow through the rotating blade row under the given law of harmonic blade oscillations is performed.

All the blades perform harmonic oscillations by the given harmonic law with a constant inter-blade phase angle (IBPA):

$$q_{ij} = q_{i0} \cdot \sin[2\pi \nu_i t + (j-1)\delta],$$

where q_{ij} is a modal coefficient ; i – the number of the natural mode; j – the blade number; q_{i0} − the amplitude of oscillations for the i –natural mode; ν_i – the natural frequency of i-mode; δ – inter-blade phase angle (IBPA) of adjacent blades.

In calculations, only one natural mode with frequency ν_1 = 120 Hz is taken into consideration.

The calculations were performed for harmonic blade oscillations at inter-blade phase angles IBPA = 0 deg, ± 90 deg, 180 deg.

The aerodynamic stability of the coupled system 'gas flow–blade row' without taking into consideration the mechanical damping is defined by the aerodynamic damping coefficient, which is equal to the performance coefficient W adopted with a minus sign, performed by the aerodynamic load, acting on the blades, during the period of oscillations

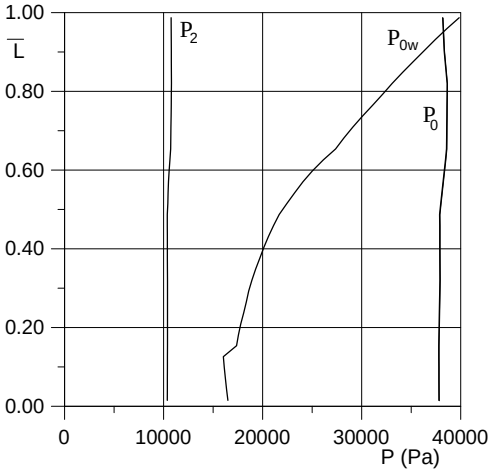

Fig. 3. Total pressure and static pressure distribution along blade length

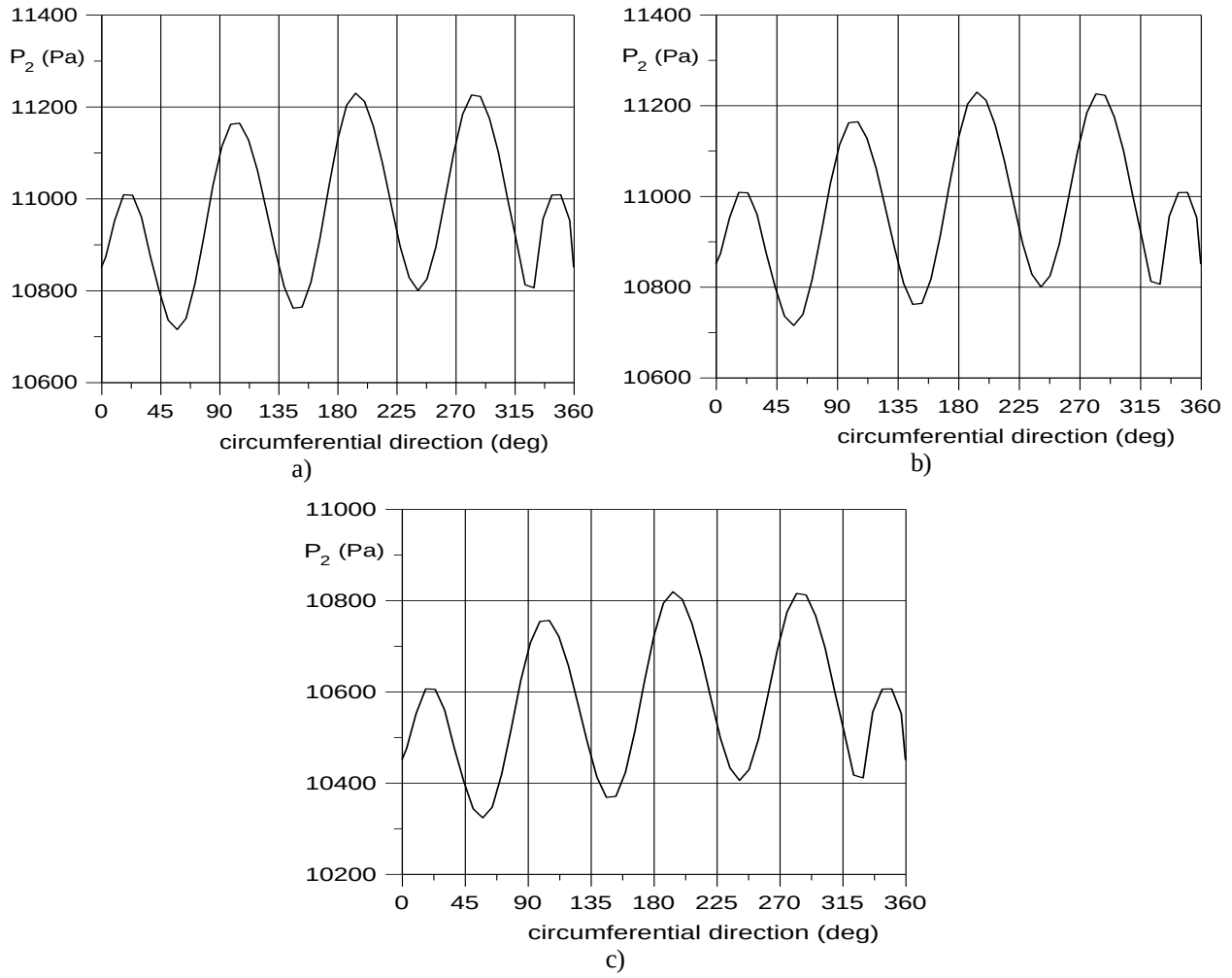

Fig. 4. Static pressure distribution behind blade row in circumferential direction
a) – root section; b) – middle section; c) – peripheral section

$$D = -W = -\int_0^{1/\nu}\int_0^{l}(F\cdot\overline{\upsilon} + M\cdot\varpi)dt\,dl\,, \tag{4}$$

where $\overline{F}$ is the aerodynamic load vector, $\overline{M}$ - the aerodynamic moment; l – the blade profile length; $\overline{\upsilon}$ - the linear velocity vector of the profile ; ϖ - the angular rotation velocity vector.

Taking into consideration the harmonic law of blade oscillations and periodical changes of the aerodynamic load from formula (4) we can obtain the expression for the aerodynamic damping coefficient

$$D = -F_0 h_0 \sin\alpha - M_0\varphi_0 \sin\beta \tag{5}$$

where F_0, M_0 are the amplitudes of the aerodynamic force and aerodynamic moment; h_0, φ_0 are the amplitudes of bending and torsional oscillations; α, β are the shift phase angles of force and moment relative to the blade bending and torsion.

It can be seen from expression (5) that if the aerodynamic force and moment signs coincide with the sign of the profile displacement and torsion, then the performance coefficient is positive ($W > 0$; $D < 0$). In this case, the energy of the main gas flow is supplied to the oscillating blade. If the aerodynamic force and moment signs are opposite to the sign of the profile displacement and torsion, then the performance coefficient is negative ($W < 0$; $D > 0$). In this case, the oscillating blade energy is dispersed in the main gas flow.

The minus sign of the performance coefficient ($D > 0$) corresponds to aerodamping, whereas the plus sign of the performance coefficient ($D < 0$) corresponds to self-excitation.

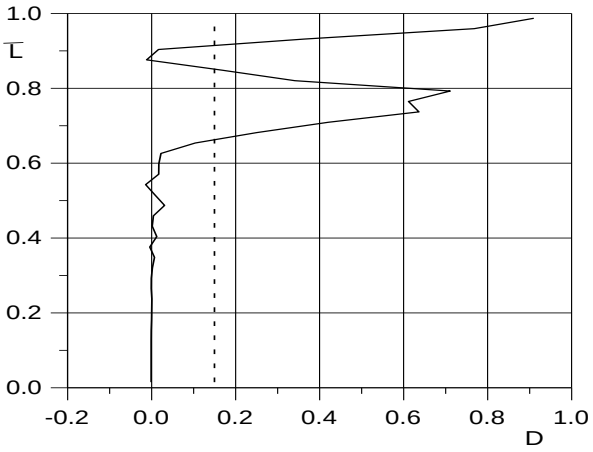

Fig. 5. Aerodamping coefficient versus blade length (the 1st mode, IBPA = 0 deg)

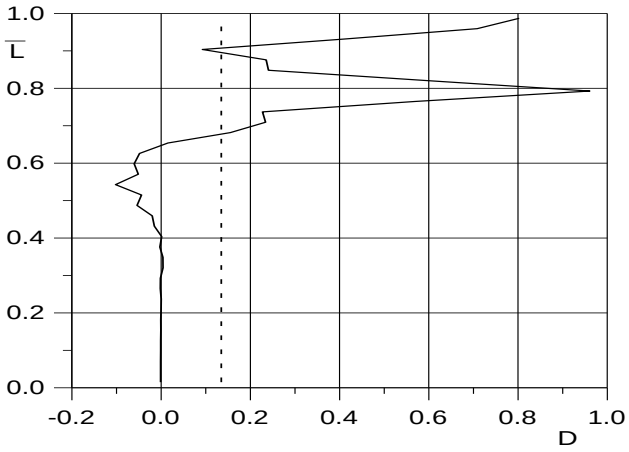

Fig. 6. Aerodamping coefficient versus blade length (the 1st mode, IBPA = 180 deg)

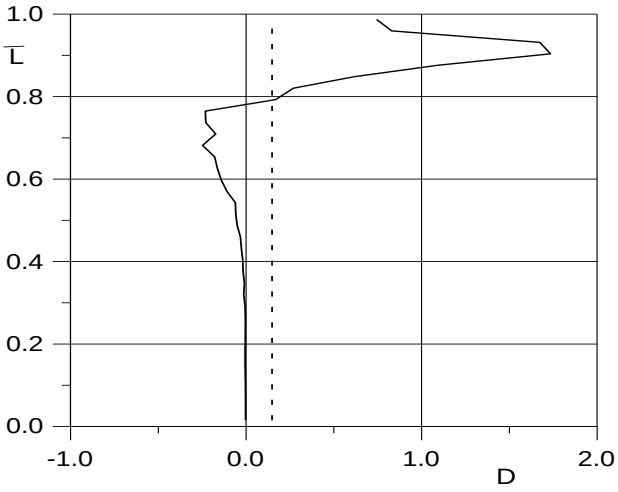

Fig. 7. Aerodamping coefficient versus blade length (the 1st mode, IBPA = -90 deg)

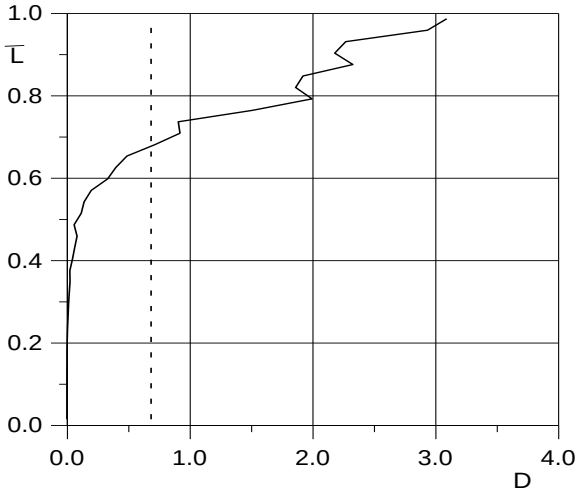

Fig. 8. Aerodamping coefficient versus blade length (the 1st mode, IBPA = +90 deg)

The energy exchange between the gas flow and the oscillating blade is depicted in Figs. 5 − 9. Figs. 5 − 8 present the graphs of the aerodamping coefficient *D* along the blade length at different values of IBPA = 0 deg; ± 90 deg; 180 deg.

The average value of the aerodamping coefficient in dependence upon the IBPA is shown in Fig. 9. We observe that the aerodamping is realized under all values of the IBPA. The minimum value of aerodamping occurs at IBPA = +90 deg.

Starting from some moment the blade displacement is defined by the unsteady forces acting on the blade, which, in its turn, depend upon the blade oscillations. We receive the coupled oscillations which depend upon the energy exchange between unsteady flow and oscillating blades.

In Figs. 10 − 12 are shown the blade peripheral section displacement in a circumferential direc-

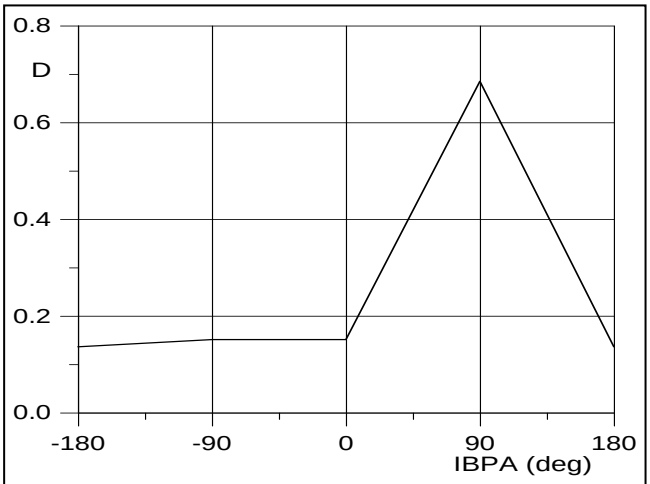

Fig.9. Average value of aerodamping coefficient versus IBPA (the 1st mode)

tion (Fig. 10), in the axial direction (Fig. 11), and the rotation angle relative to the gravity center (Fig. 12) for IBPA = 0 deg. In Figs. 10, a − 12, a are presented the graphs of displacement during the 10 periods of coupled oscillations, in Figs. 10, b − 12, b are presented the graphs of the amplitude-frequency spectrum of blade oscillations. As it follows from the graphs the blade oscillations are damped.

In Figs. 13 − 21 are presented the graphs of aerodynamic loads (circumferential force, axial force and aerodynamic moment) acting on the root, middle and peripheral blade layers for IBPA = 0 deg during the 10 periods of oscillations (Fig. 13, a − 21, a) and the amplitude-frequency spectrum (Fig. 13, b − 21, b).

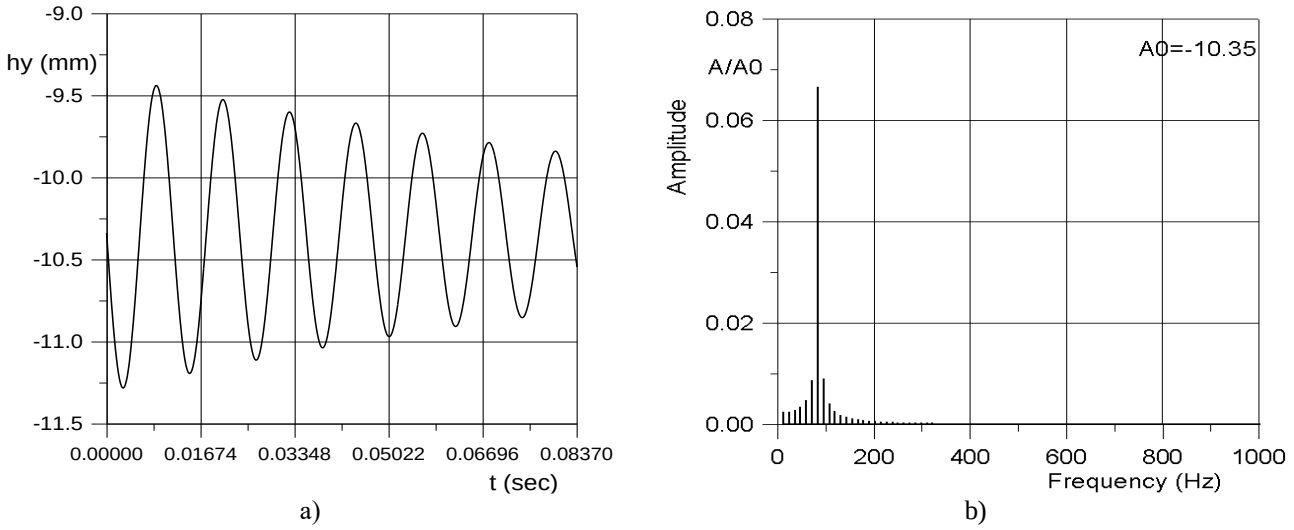

a) b)

Fig.10. Peripheral section displacement in circumferential direction (1st mode, IBPA = 0 deg):
a) − displacement during the 10 periods; b) − amplitude-frequency spectrum

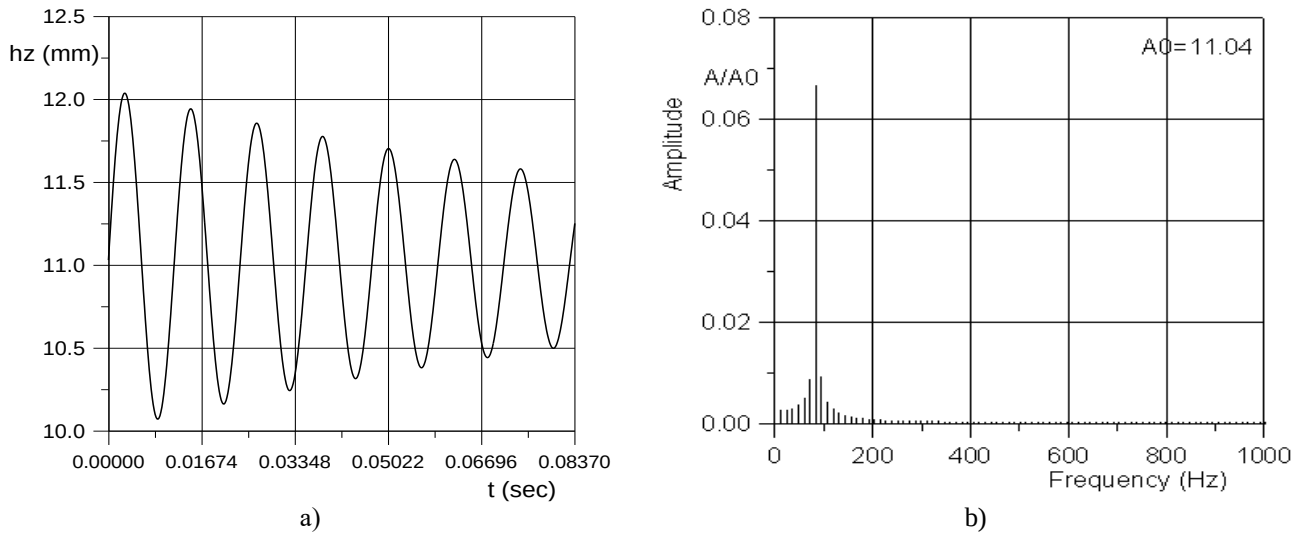

a) b)

Fig. 11. Peripheral section displacement in axial direction (1st mode, IBPA=0 deg):
a) − displacement during the 10 periods; b) − amplitude-frequency spectrum

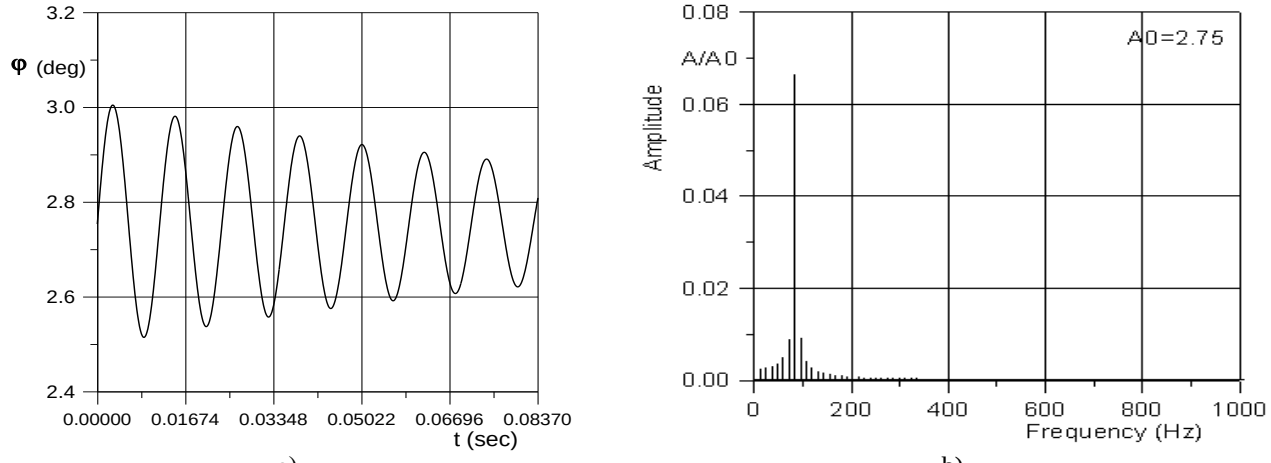

a) b)

Fig. 12. Peripheral section rotation (1st mode, IBPA = 0 deg):
a) − rotation during the 10 periods; b) − amplitude-frequency spectrum

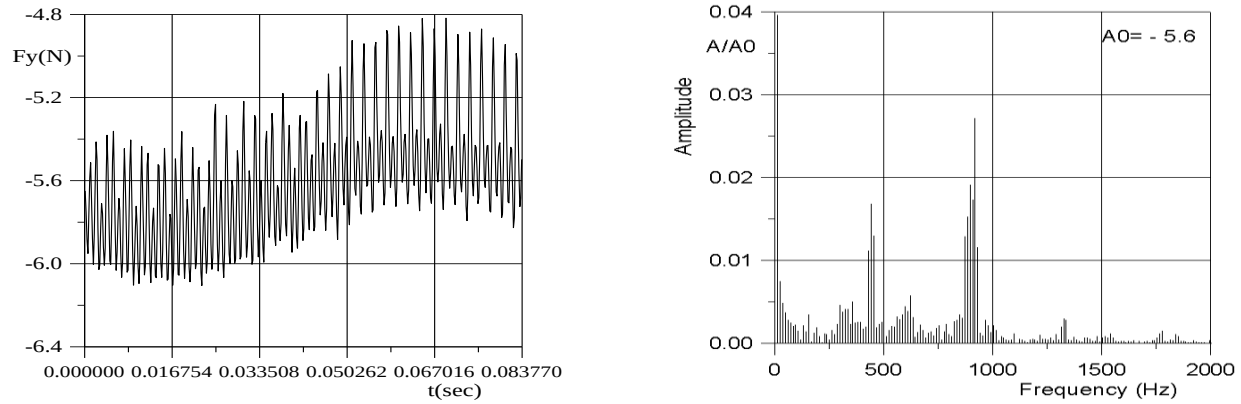

a) b)

Fig. 13. Circumferential force acting on turbine rotor blade root layer (1st mode, IBPA = 0 deg):
a) − circumferential force during the 10 periods of coupled oscillations; b) − amplitude-frequency spectrum

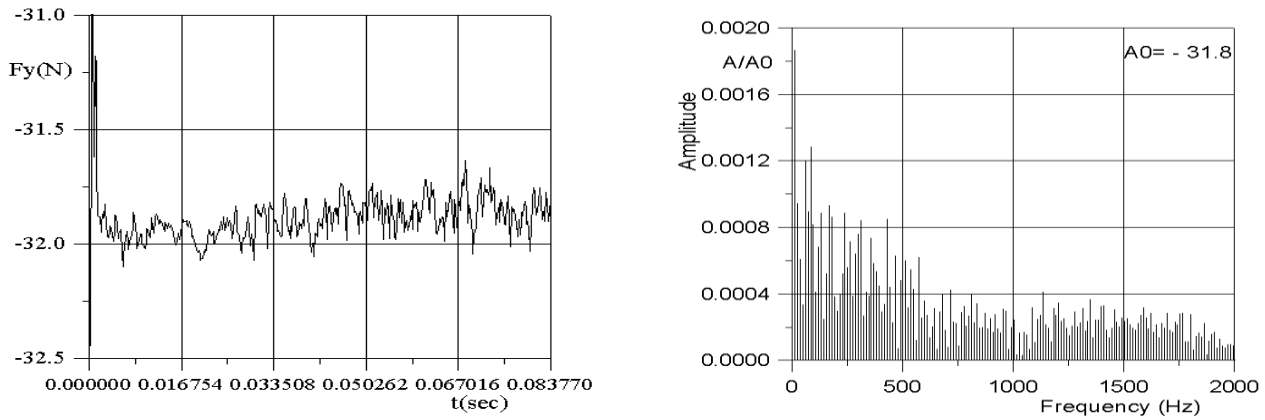

a) b)

Fig. 14. Circumferential force acting on turbine rotor blade middle layer (1st mode, IBPA = 0 deg):
a) − circumferential force during the 10 periods of coupled oscillations; b) − amplitude-frequency spectrum

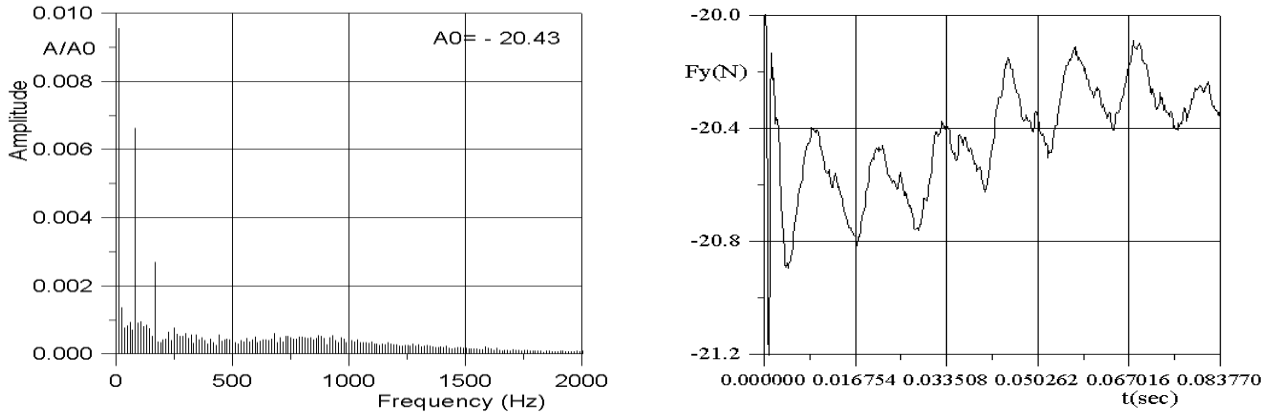

a) b)

Fig. 15. Circumferential force acting on turbine rotor blade peripheral layer (1st mode, IBPA = 0 deg):
a) − circumferential force during the 10 periods of coupled oscillations; b) − amplitude-frequency spectrum

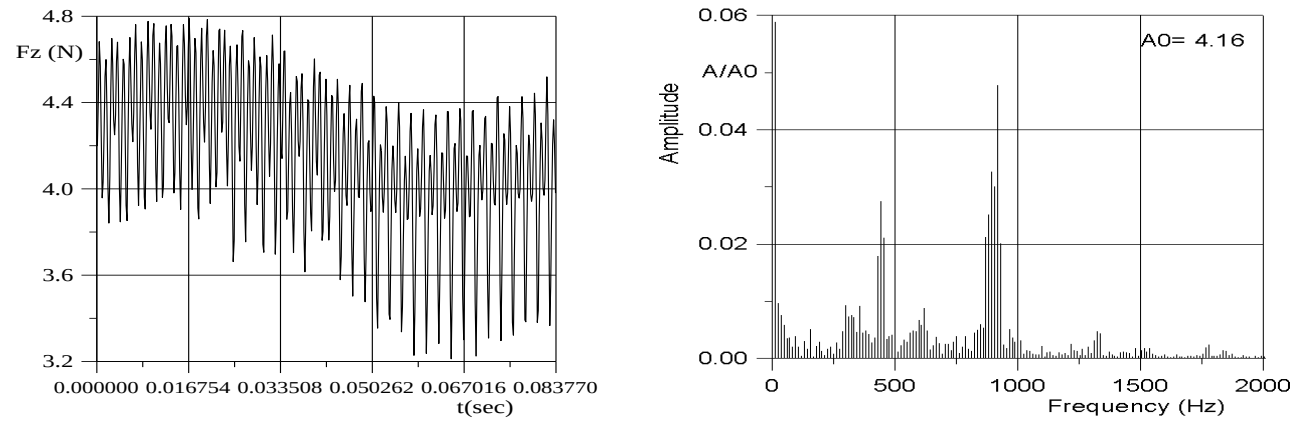

a) б)

Fig. 16. Axial force acting on turbine rotor blade root layer (1st mode, IBPA = 0 deg):
a) − axial force during the 10 periods of coupled oscillations; b) − amplitude-frequency spectrum

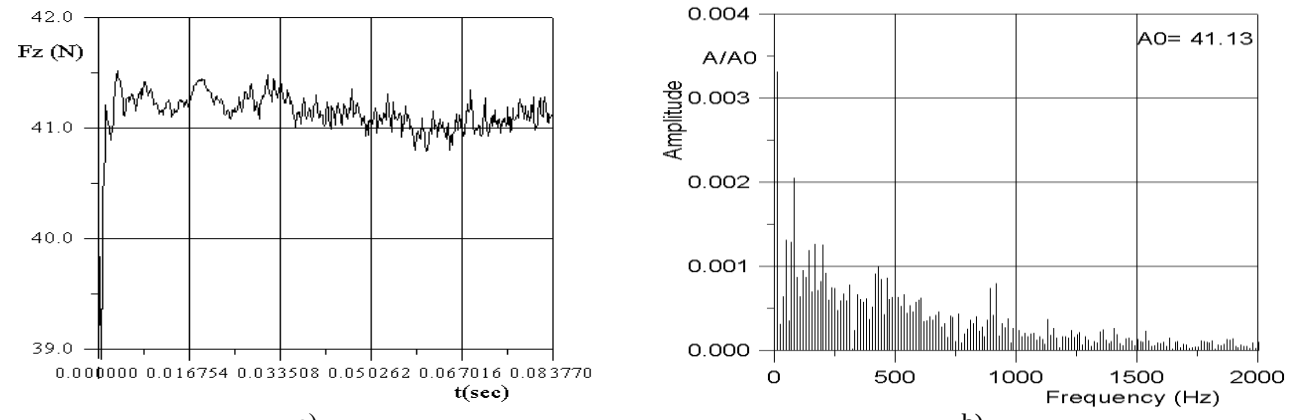

a) b)

Fig. 17. Axial force acting on turbine rotor blade middle layer (1st mode, IBPA = 0 deg):
a) − axial force during the 10 periods of coupled oscillations ; b) − amplitude-frequency spectrum

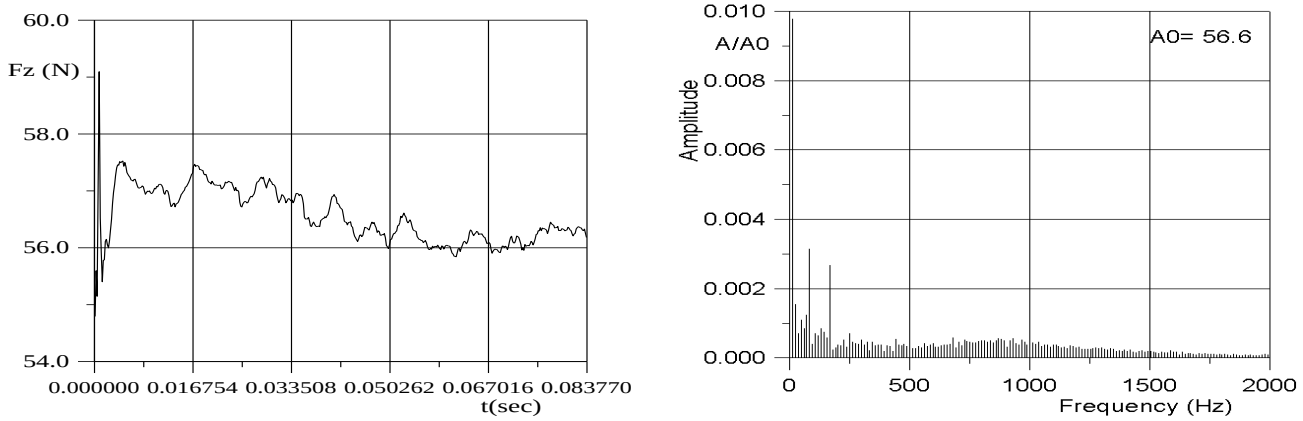

a) b)

Fig. 18. Axial force acting on turbine rotor blade peripheral layer (1st mode, IBPA = 0 deg):
a) − axial force during the 10 periods of coupled oscillations; b) − amplitude-frequency spectrum

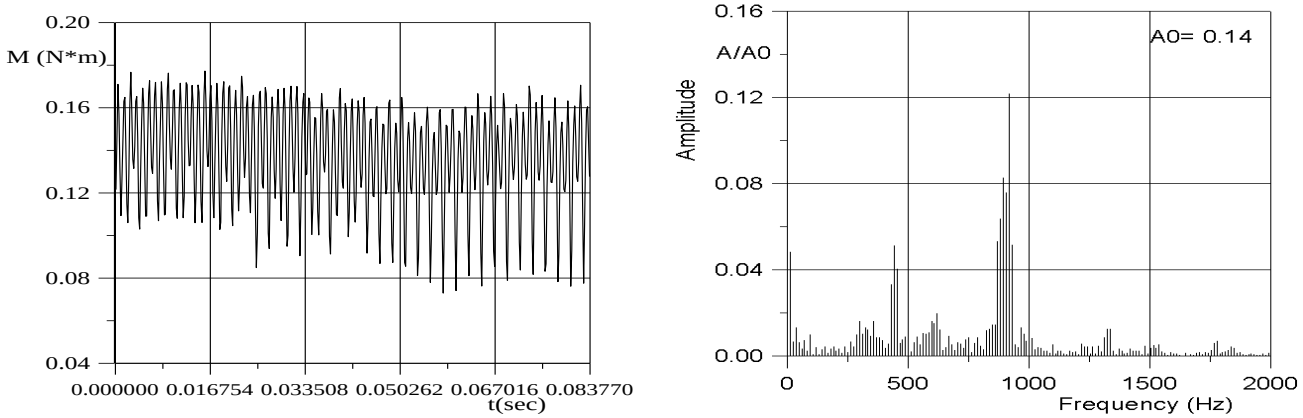

a) б)

Fig. 19. Aerodynamic moment acting on turbine rotor blade root layer (1st mode, IBPA = 0 deg):
a) − aerodynamic moment during the 10 periods of coupled oscillations; b) − amplitude-frequency spectrum

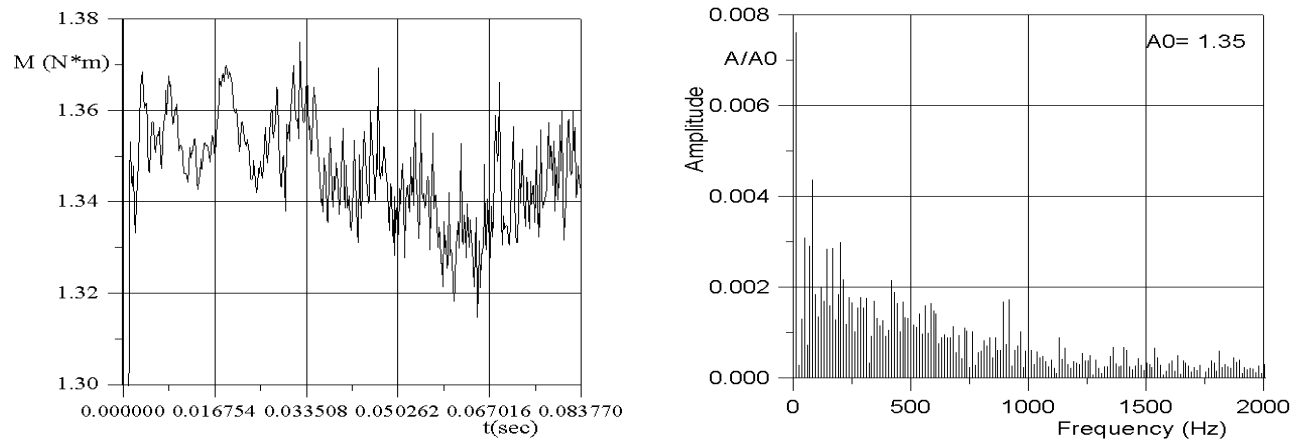

a) б)

Fig. 20. The aerodynamic moment acting on turbine rotor blade mid layer (1st mode, IBPA = 0 deg):
a) −aerodynamic moment during the 10 periods of coupled oscillations; b)−amplitude-frequency spectrum

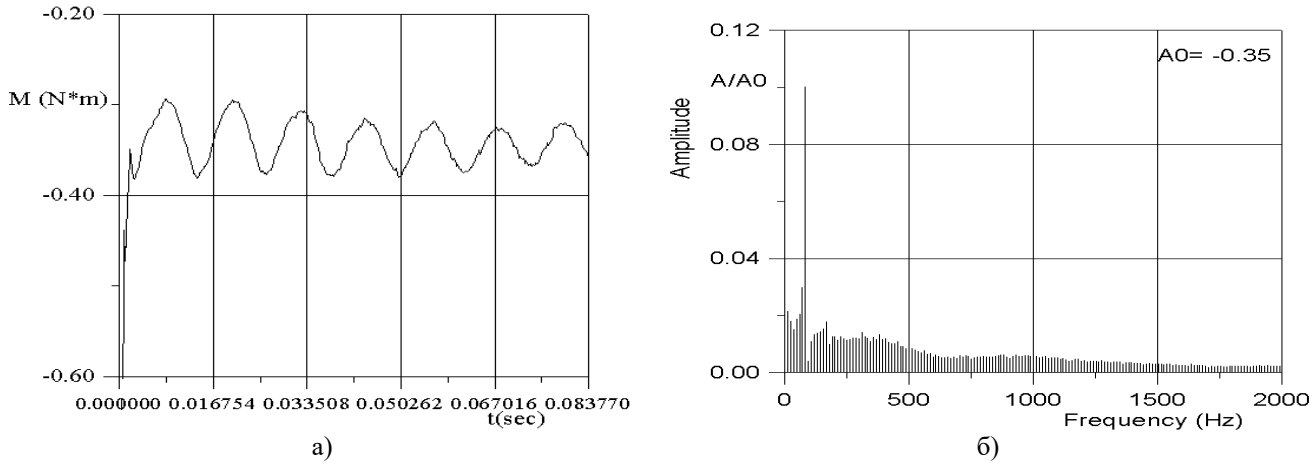

а) б)

Fig. 21. Aerodynamic moment acting on turbine rotor blade peripheral layer (1st mode, IBPA = 0 deg):
a) − aerodynamic moment during the 10 periods of coupled oscillations; b) − amplitude-frequency spectrum

Conclusion

The numerical method for integrating the 3D Reynolds-averaged Navier-Stokes (RANS) equations with the modified Baldwin and Lomax algebraic turbulence eddy viscosity model is applied to calculate 3D unsteady viscous flow through a steam turbine rotor blade row.

The graphs of blade displacement and the aerodynamic loads acting on the blade for coupled oscillations at IBPA = 0 deg.

The proposed numerical method can be applied to predict the aeroelastic behaviour of the last stages of the rotor blade rows for axial steam and gas turbines and compressors [1, 3–7].

References

1. Gnesin V., Rzadkowski R., Kolodyazhnaya L. Coupled Fluid-Structure Problem for 3D Transonic Flow Through a Turbine Stage with Oscillating Blades. *Aerothermodynamic of Internal Flows:* Proc. of 5th Intern. Symp. On Exper. and Comput. (Gdansk, Poland, 4–7 Sept. 2001). Gdansk. 2001. P. 275–284.
2. Baldwin B., Lomax H. Thin layer approximation and algebraic model for separated turbulent flow. *AIAA Paper 78–0257*. 1978. P. 1−45.
3. Gnesin V., Rzadkowski R., Kolodyazhnaya L. Numerical Modelling of fluid–structure interaction in a turbine stage for 3D viscous flow in nominal and off−design regimes. *ASME. TURBO-EXPO 2010, GT2010−23779*, Glasgow, UK. 2010. P. 1−9.
4. Gnesin V. I., Kolodyazhnaya L. V. Numerical Modelling of Aeroelastic Behaviour for Oscillating Turbine Blade Row in 3D Transonic Ideal Flow. *J. Problems in Mash. Eng.* 1999. Vol. 1. No. 2. P. 65–76.
5. Gnesin V. I., Kolodyazhnaya V. L., Rzadkowski R. A numerical modelling of stator-rotor interaction in a turbine stage with oscillating blades. *J. Fluid and Structure.* 2004. No. 19. P. 1141–1153.
6. Rzadkowski R., Gnesin V. I., Kolodyazhnaya L. V. Rotor Blade Flutter in Last Stage of LP Steam Turbine. *Aerodynamics, Aeroacoustics & Aeroelasticity of Turbomachines ISUAAAT14 8-11*: Proc. of the 14th Intern. Symp. on Unsteady, (Stockholm, Sweden, Sept. 2015). Stockholm. 2015. I14-S1-4. P. 1–6.
7. Gnesin V. I. Aeroelastic Phenomena in Turbomachines / Gnesin V. I., Kolodyazhnaya L. V. // Aerodynamics and Aeroacoustics: Problems and Perspectives. – 2009. – No 3. – P. 53–62.

Received 24 January 2018